Ab initio molecular dynamics simulations of the static, dynamic, and electronic properties of liquid Pb using real-space pseudopotentials

M. M. G. Alemany, R. C. Longo, and L. J. Gallego
Departamento de Física de la Materia Condensada, Facultad de Física, Universidad de Santiago de Compostela, E-15782 Santiago de Compostela, Spain

D. J. González and L. E. González
Departamento de Física Teórica, Facultad de Ciencias, Universidad de Valladolid, E-47011 Valladolid, Spain

Murilo L. Tiago
Materials Science and Technology Division, Oak Ridge National Laboratory, Oak Ridge, Tennessee 37831, USA

James R. Chelikowsky
Center for Computational Materials, Institute for Computational Engineering and Sciences, Departments of Physics and Chemical Engineering, University of Texas, Austin, Texas 78712, USA

(Received 7 August 2007; revised manuscript received 2 October 2007; published 13 December 2007)

We performed a comprehensive study of the static, dynamic, and electronic properties of liquid Pb at $T=650$ K, $\rho=0.0309$ Å^{-3} by means of 216-particle *ab initio* molecular dynamics simulations based on a real-space implementation of pseudopotentials constructed within density-functional theory. The predicted results and available experimental data are in very good agreement, which confirms the adequacy of this technique to achieve a reliable description of the behavior of liquid metals, including their dynamic properties. Although some of the computed properties of liquid Pb are similar to those of simple liquid metals, others differ markedly. Our results show that an appropriate description of liquid Pb requires the inclusion of relativistic effects in the determination of the pseudopotentials of Pb.

DOI: 10.1103/PhysRevB.76.214203 PACS number(s): 61.25.Mv, 61.20.Ja, 71.15.Pd

I. INTRODUCTION

Molecular dynamics (MD) is a powerful simulation technique for describing the properties of condensed matter systems in general and, in particular, those of liquid metals. MD results allow the assessment of the reliability of available theoretical approximations, also affording information on properties that would be very difficult or impossible to determine experimentally or simply have not been measured. MD simulations fall into two broad classes. One is classical MD (CMD) simulations, in which the simulated particles are moved in accordance with the dictates of some interatomic potentials. In CMD, the electronic degrees of freedom are not explicitly treated. The second class of MD simulations is based on *ab initio* MD (AIMD) simulations using quantum forces between the nuclei. In AIMD, these forces are computed using electronic structure calculations that are performed as the MD trajectory is generated. In recent years, there has been a marked increase in the use of AIMD methods based on density-functional theory (DFT).[1,2] For a specified set of nuclear positions, the Hellmann-Feynman theorem[3] is employed to obtain the forces acting on the nuclei following the calculation of the ground-state density and energy of the valence electrons. In DFT-based AIMD simulations, the nuclear positions thus evolve in accordance with classical mechanics, while the valence electron subsystem follows adiabatically, i.e., the system remains on the Born-Oppenheimer surface.

Liquid lead (l-Pb) is an intriguing system that has been the subject of theoretical, experimental, and MD investigations. Some theoretical investigations used semiempirical approaches based on the simple hard-sphere (HS) model to calculate a number of properties. For instance, Ashcroft and Lekner[4] used the HS packing fraction as a fitting parameter to obtain fairly good description of the static structure factor $S(q)$ of l-Pb, which combined with pseudopotential theory and Ziman's formula[5] afforded a reasonable estimate of the electrical resistivity. A similar approach was followed by Umar and Young,[6] who calculated the HS packing fraction within the framework of a variational theory based on the Gibbs-Bogoliubov inequality. This scheme gave a good estimate of $S(q)$ both at $T=613$ K (near the melting point, $T=600.61$ K) and at a higher temperature ($T=1373$ K). The HS model was also used by Ascarelli[7] to achieve reasonable predictions of the isothermal compressibility K_T, the speed of sound c_s, and their temperature dependencies.

The static structure and some dynamic properties of l-Pb were computed by Mentz-Stern and Hoheisel[8] by CMD simulations using a six-center Lennard-Jones pair potential to model the atomic interactions. At $T=615$ K, $S(q)$ was found to be in fair agreement with experiment, i.e., the main peak was slightly lower than the experimental data and the subsequent oscillations were somewhat out of phase. However, the calculated self-diffusion D and shear viscosity η were approximately 30% smaller and 20% greater, respectively, than the experimental values. CMD simulations, with interactions described by a pair potential $\Phi(r)$ derived from a nonlocal pseudopotential with relativistic core functions, were performed by Jank and Hafner[9] to study the structural and electronic properties of l-Pb at $T=619$ K. Their com-

puted atomic structure showed rather good agreement with experimental data, i.e., the main peak of the pair distribution function $g(r)$ was slightly shifted to greater r values, and the main peak of $S(q)$ was around 18% higher than the experimental values. Their calculated electronic density of states (DOS) suggested a metallic behavior, although strongly departing from that of a free-electron system and showing a marked gap at approximately 5.0 eV below the Fermi level. The results by Jank and Hafner highlighted the importance of using relativistic core functions in the determination of the Pb pseudopotential. They found a nonrelativistic pseudopotential that gave rise to a $\Phi(r)$ with a repulsive core plus an oscillatory tail (Friedel oscillations), whereas the inclusion of relativistic corrections induced a strong damping of the oscillatory tail, leading to a $\Phi(r)$ which practically reduces to a purely repulsive core. Dzugutov *et al.*[10] investigated the static and dynamic properties of l-Pb using an effective pair potential which was derived from a fit to the experimental static structure factor $S(q)$, in conjunction with CMD simulations along with advanced liquid state theories. Their work provided useful insights into some time correlation functions and their associated memory functions, and, more importantly, it was helpful for assessing the range of validity of the mode-coupling theory. Using also CMD simulations, Bryk and Mryglod[11] investigated the collective dynamics of l-Pb in terms of generalized collective modes. They found that, beyond the hydrodynamic region, the spectrum of the collective excitations had three pairs of kinetic propagating modes in addition to the generalized sound modes.

Recently, the static and electronic properties of l-Pb have been investigated by AIMD methods.[12–14] The first of such studies was performed by Kresse,[12] who computed the static structure of l-Pb near the triple point using the Vienna *ab initio* simulation package (VASP)[15] with 96 particles and the generalized gradient approximation for the exchange and correlation potential.[16] $S(q)$ was found to have a too pronounced main peak and the depth of the subsequent minimum was also overestimated. Similar issues appeared in $g(r)$, with oscillations being somewhat out of phase. These inaccuracies were attributed by Kresse[12] to the small system size and the low temperature (T=610 K) used in the simulations. A better description of the static structure of l-Pb was obtained by Knider *et al.*,[14] who calculated $g(r)$ near the triple point by means of 32-particle AIMD simulations using the SIESTA code.[17] Knider *et al.*[14] also calculated electronic properties such as the dc conductivity and the DOS, which showed similar features to those obtained by Jank and Hafner[9] by CMD simulations.

With regard to the experimental information on l-Pb, its static structure has been determined by means of x-ray (XR)[18] and neutron scattering (NS)[19–21] measurements at several temperatures within the range 613–1163 K. $S(q)$ always showed a symmetrical main peak along with other features typical of simple liquid metals. This explains why the static structure can be fairly well described using the simple HS model.[4,6] The first experiments on the dynamic structure of l-Pb by inelastic NS (INS) techniques were carried out in the 1950s.[22,23] Later, in the 1980s, Söderström *et al.*[24–27] performed new INS measurements at T=623 and 1173 K. For both states, data were collected over a similar range of momentum transfers. For instance, at T=623 K, the data covered the range $0.18q_p \leqslant q \leqslant 3.0q_p$ [$q_p \sim 2.20$ Å^{-1} is the position of the main peak of $S(q)$]. These experimental measurements provided evidence of the existence of collective excitations in l-Pb up to $q \sim 3/5q_p$, which basically coincides with what has been found in simple liquid metals.[28–32] However, it was not possible to ascertain the possible existence of a "positive dispersion" effect, as it would require to collect data up to much smaller q values.

In this paper, we present the results of a comprehensive study of the static, dynamic, and electronic properties of l-Pb by means of 216-particle AIMD simulations based on PARSEC, a DFT-based pseudopotential algorithm for real-space electronic structure calculations.[33] Our calculations were carried out with the two following objectives: (a) to obtain a good description of the behavior of l-Pb through AIMD simulations and (b) to examine in detail, within the theoretical framework employed in this work, the importance of including relativistic effects in the pseudopotentials of Pb for an accurate description of l-Pb properties.

In Sec. II, we describe the AIMD method used in this work. In Sec. III, we discuss our results comparing them with available experimental data. Finally, in Sec. IV, we summarize our main conclusions.

II. COMPUTATIONAL METHOD

One of the most successful ways in obtaining the electronic structure of matter has been the use of computational approaches based on DFT. Among these approaches, real-space pseudopotential techniques[34] have recently attracted special interest owing to their computational advantages, especially the ease of implementation. Pseudopotential theory allows one to focus on the chemically active valence electrons by replacing the strong all-electron atomic potential by a weak pseudopotential, which effectively reproduces the effects of the core electrons on the valence states. This approximation significantly reduces the number of eigenpairs to be handled, especially for heavier elements. Since the energy and length scales are set by the valence states, simple bases can be used. Working in real space has a number of points in its favor. Implementation of these approaches is simple: there is no "formal" basis. As for plane waves, the "grid basis" is independent of the atomic positions, and only one parameter, the spacing of the grid, needs to be refined to control convergence. (The equivalent parameter in plane waves is the energy "cutoff" parameter.) Second, real-space methods are semilocal, which facilitates implementation on parallel computers. This makes such methods highly attractive for computation of the electronic structure of large, complex systems.

In this work, we adopted a real-space pseudopotential approach to study l-Pb. Specifically, we performed AIMD simulations using the PARSEC code.[33] In this method, the Kohn-Sham equations are solved self-consistently on a cubic three-dimensional real-space grid within a supercell geometry.[35] The core electrons were represented by norm-conserving pseudopotentials generated for the reference con-

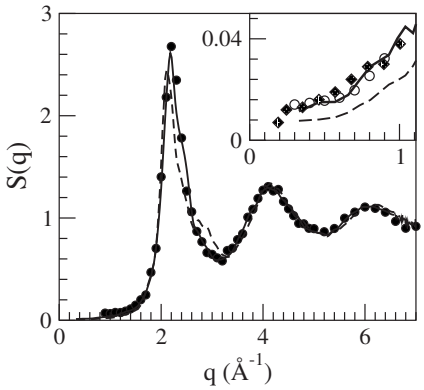

FIG. 1. Static structure factor $S(q)$ for l-Pb. The solid and dashed lines represent our AIMD results at $T=650$ K using relativistic and nonrelativistic pseudopotentials, respectively, and the solid circles represent the experimental NS data at $T=643$ K (Ref. 20). The inset shows low-q AIMD results, which are compared with XR (open circles, Ref. 18) and NS (solid diamonds, Ref. 21) data near melting.

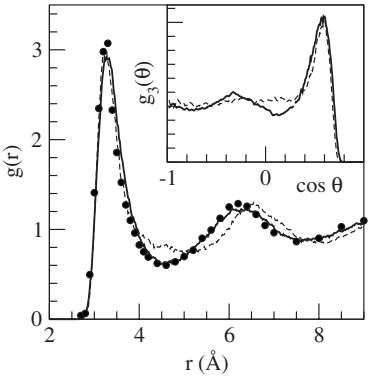

FIG. 2. Pair distribution function $g(r)$ for l-Pb. The solid and dashed lines represent our AIMD results at $T=650$ K, using relativistic and nonrelativistic pseudopotentials, respectively, and the solid circles represent the experimental XR data near melting (Ref. 18). The inset shows the computed bond angle distribution, $g_3(\theta)$.

figuration $[\mathrm{Xe}]6s^2(5f^{14}5d^{10})6p^26d^0$ using the Troullier-Martins prescription,[36] with a radial cutoff of 3.2 a.u. (1 a.u.=0.529 Å) for the s, p, and d channels. The potential was made separable by the procedure of Kleinman and Bylander,[37] applied in real space, with the p potential chosen to be the local component. A partial-core correction for nonlinear exchange correlation was included in the pseudopotential construction. The local density functional of Ceperley and Alder[38] was used as parametrized by Perdew and Zunger,[39] and the single Γ point was employed in sampling the Brillouin zone. A spacing of 0.65 a.u. was used for constructing the real-space grid.

Calculations were performed for a thermodynamic state of l-Pb characterized by the number density $\rho=0.0309$ Å^{-3} and the temperature $T=650$ K (~50 K above the measured melting point). 216 atoms were placed at random in a cubic supercell; the cell was coupled to a virtual heat bath via the Langevin equation of motion[40] and was heated far above the target temperature in order to eradicate any memory of its initial configuration. The temperature was then set to 650 K; the system allowed to stabilize, and gradually decoupled from the virtual heat bath. Then, an AIMD simulation run was performed over 1000 time steps (5 ps of simulated time), ion dynamics being generated using the Beeman algorithm[41] with Hellmann-Feynman forces.[3] Previously, an equilibration run of 1 ps was performed with the particles' velocities being rescaled so as to move the system at the desired temperature. The data from the longer simulation run were used in calculating the static, dynamic, and electronic properties reported below. Data were collected using both relativistic and nonrelativistic pseudopotentials.

III. RESULTS AND DISCUSSION

A. Static properties

Figure 1 (continuous line) shows the static structure factor $S(q)$ obtained in our AIMD simulations of l-Pb at $T=650$ K using pseudopotentials with relativistic corrections. The main characteristic is the existence of a very symmetrical main peak located at ~2.19 Å^{-1}. The computed $S(q)$ agrees very well with the NS data obtained by Dahlborg *et al.*[20] at $T=643$ K for the whole q range. An additional comparison with experiment is provided in the inset of Fig. 1, which is focused on the low-q region. Within this region, very good agreement also exist between the AIMD results and the experimental XR (Ref. 18) and NS (Ref. 21) data near melting. Extrapolation of $S(q)$ to $q\rightarrow 0$ allows the isothermal compressibility K_T to be estimated from the relation $S(q\rightarrow 0)=\rho k_B T K_T$, where k_B is the Boltzmann constant. A least squares fit of $S(q)=s_0+s_2q^2$ to the computed $S(q)$ for q values up to 0.7 Å^{-1} yields the result $S(q\rightarrow 0)=0.010$, thus yielding the value $K_T=3.60$ (in units of 10^{-11} m^2 N^{-1}). This result is close to the experimental data taken near melting, $K_T=3.49$.[42]

Closely related to $S(q)$ is the pair distribution function $g(r)$, which provides information about the short range order in the liquid. Figure 2 (continuous line) shows the calculated $g(r)$, which has a main peak at 3.28 Å and closely follows the corresponding experimental values.[18] This result clearly improves on that obtained in Kresse's AIMD study of l-Pb using VASP,[12] where $g(r)$ had the main peak somewhat shifted to greater r values and slightly overestimated the amplitude of the following oscillations. To evaluate the coordination number N_c in l-Pb, we integrate $4\pi r^2 g(r)$ up to the position of its first minimum (which corresponds to the value $R_{min}=4.40$ Å), obtaining $N_c\sim 11.3$. The bond angle distribution function $g_3(\theta)$ gives information about the distribution of bond angles defined by atoms up to a distance which we have taken as R_{min}. The calculated $g_3(\theta)$, shown in the inset of Fig. 2 (continuous line), exhibits two distinct peaks at ~58° and 108°. These features, including the value obtained for N_c, are rather close to those of a system with local icosahedral structure, which is typical of simple liquid metals near melting.[30]

Figure 1 (dashed line) shows the static structure factor $S(q)$ obtained using pseudopotentials that do not include

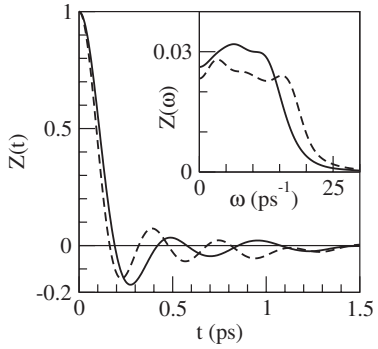

FIG. 3. Normalized velocity autocorrelation function $Z(t)$ for l-Pb at $T=650$ K, as obtained from our AIMD simulations. The solid line is for the relativistic pseudopotentials and the dashed line for the nonrelativistic pseudopotentials. The inset shows the corresponding power spectrum $Z(\omega)$.

relativistic corrections. A substantial modification of the previously determined $S(q)$ is found, the agreement with experimental data being less satisfactory in this case. $S(q)$ has a remarkably asymmetrical main peak along with a broad shoulder at its high-q side. [We note that such a shoulder is a characteristic feature of the behavior of $S(q)$ for the other, lighter, molten group IV elements Si, Ge, and Sn; see, e.g., Ref. 12.] The influence of not including relativistic effects in the Pb pseudopotentials is also apparent in the other structural quantities, $g(r)$ and $g_3(\theta)$, that are shown in Fig. 2. The oscillations in $g(r)$ are now dampened and the coordination number becomes $N_c \sim 10.1$ atoms (with $R_{min}=4.21$ Å). The bond angle distribution becomes more structureless, which indicates an increased diversity in the local order.

The results presented above show that the inclusion of relativistic effects in the pseudopotentials of Pb is necessary for an accurate description of the static properties of l-Pb through DFT-based AIMD simulations. As shown below, the same holds for the dynamic and electronic properties.

B. Dynamic properties

1. Single particle dynamics

Figure 3 shows the results obtained for the normalized velocity autocorrelation function $Z(t)$, calculated as

$$Z(t) = \frac{\langle \mathbf{v}_a(t) \cdot \mathbf{v}_a(0) \rangle}{\langle \mathbf{v}_a(0) \cdot \mathbf{v}_a(0) \rangle}, \tag{1}$$

where $\mathbf{v}_a(t)$ is the velocity of a tagged ion in the fluid and angle brackets indicate an ensemble average. $Z(t)$ exhibits the backscattering and other features typical of simple liquid metals near melting.[28–30,43,44] The deepness of the first minimum (when relativistic corrections are taken into account) is around 0.27 ps and the subsequent maximum has a rather small amplitude. The self-diffusion coefficient D was found to be 0.21 ± 0.02 Å^2/ps when calculated as the time integral of $Z(t)$ and 0.22 ± 0.02 Å^2/ps when calculated as the slope of the mean square ion displacement function $\Delta R^2(t) \equiv \langle |\mathbf{R}_a(t) - \mathbf{R}_a(0)|^2 \rangle$. These results are very close to the experimental data obtained by Tanigaki *et al.*[45] at $T=645$ K, 0.235 ± 0.005 Å^2/ps. The power spectrum of $Z(t)$, $Z(\omega)$, shown in the inset of Fig. 3, exhibits a two-peaked shape, which is typical of simple liquid metals near melting.[28–30]

Figure 3 shows that the use of nonrelativistic pseudopotentials induces visible changes in the predicted single particle dynamics of l-Pb. First, $Z(t)$ has a steeper decay and, after taking negative values, it reaches its minimum at a short time. This is understandable in terms of the so-called "cage effect",[43,46,47] by which a given particle rebounds against the cage formed by its nearest neighbors. As the cage's size is proportional to $R_{\min}$, when relativistic effects are not taken into account, the cage is smaller and the particle rebounds sooner. The short time expansion of $Z(t)$ reads $Z(t)=1-\omega_E^2 t^2/2+\ldots$, where ω_E is the so-called "Einstein frequency" of the system, and provides an estimate of the frequency at which a given particle is vibrating within the cage.[29] A sort time fitting of the two $Z(t)$ curves in Fig. 3 yields the values $\omega_E \sim 10.0$ and 12.0 ps^{-1} for the relativistic and nonrelativistic pseudopotentials, respectively. In both cases, the corresponding ω_E falls among the two peaks of the associated $Z(\omega)$, which is another feature typical of simple liquid metals.[28–30] The self-diffusion coefficient corresponding to the nonrelativistic pseudopotentials is 0.18 ± 0.02 Å^2/ps, which differs somewhat from the experimental data indicated above.

2. Collective dynamics

The collective dynamics of density fluctuations in the liquid is usually described by means of the intermediate scattering function $F(q,t)$, defined as

$$F(q,t) = \frac{1}{N}\left\langle \sum_{l,m} \exp\{-i\mathbf{q} \cdot [\mathbf{R}_l(t) - \mathbf{R}_m(0)]\} \right\rangle, \tag{2}$$

where N is the total number of atoms and $\mathbf{R}_l(t)$ is the position of the lth atom at time t. The time Fourier transform (FT) of $F(q,t)$ into the frequency domain gives the dynamic structure factor $S(q,\omega)$, which is directly related to the intensity of scattering in INS or inelastic x-ray experiments.

In our AIMD simulations, $F(q,t)$ was found to oscillate up to $q \sim (3/5)q_p = 1.4$ Å^{-1}, the amplitude of the oscillations being stronger for the smaller q values (Fig. 4). This behavior is typical of simple liquid metals near melting, as has been found by computer simulations[31,46,49,50] and theoretical models.[51] However, at low-q values ($q \leqslant 0.5q_p$), $F(q,t)$ shows an appreciable diffusive component that imposes a slow decay. This is at variance with the results obtained for simple liquid metals (alkalis, alkali earths, and Al) near melting,[31,46,49–51] where for a comparable q range the diffusive component is already very weak and the corresponding $F(q,t)$ shows marked oscillations around zero. This difference can be understood by resorting to the following expressions of $F(q,t)$ and its corresponding $S(q,\omega)$, which are exact in the limit $q \to 0$ (hydrodynamic limit[29]):

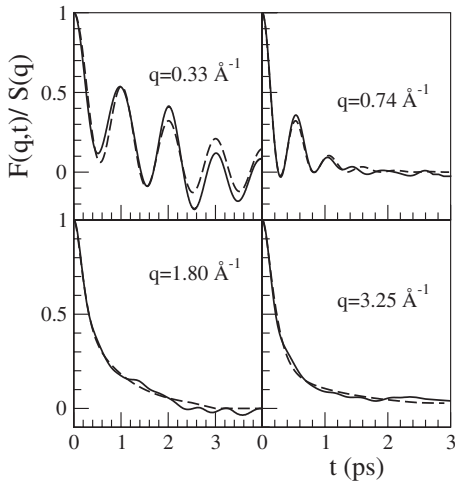

FIG. 4. Normalized intermediate scattering function, $F(q,t)/S(q)$, for *l*-Pb at $T=650$ K, as obtained from our AIMD simulations using relativistic pseudopotentials, for several values of q (solid lines). The dashed lines are the results obtained using the eight-parameter analytical expression proposed by Ebbsjo *et al.* (Ref. 48) (see below).

$$F(q,t)/S(q) = \left(\frac{\gamma-1}{\gamma}\right)\exp[-D_T(q)t] + \frac{1}{\gamma}\exp[-\Gamma(q)t] \times[\cos(c_s q t) + bq\,\sin(c_s q t)] \tag{3}$$

and

$$2\pi S(q,\omega)/S(q) = \left(\frac{\gamma-1}{\gamma}\right)\frac{2D_T(q)}{\omega^2+[D_T(q)]^2} + \frac{1}{\gamma}\left\{\frac{\Gamma(q)+bq(\omega+c_s q)}{(\omega+c_s q)^2+[\Gamma(q)]^2} + \frac{\Gamma(q)+bq(\omega-c_s q)}{(\omega-c_s q)^2+[\Gamma(q)]^2}\right\}. \tag{4}$$

Here, $\gamma=C_p/C_v$ (the ratio of specific heats); $D_T(q)=D_T q^2$, where $D_T=\kappa_T/(\rho C_p)$ is the thermal diffusivity and κ_T the thermal conductivity; $\Gamma(q)=\Gamma q^2$, Γ being the sound attenuation constant given by $\Gamma=\frac{1}{2}[a(\gamma-1)/\gamma+\nu_l]$, with $a=\kappa_T/(\rho C_v)$ and ν_l the kinematic longitudinal viscosity. According to Eq. (4), in the hydrodynamic limit, $S(q,\omega)$ has two (inelastic) propagating peaks centered at $\omega=\pm c_s q$, each one having a half width at half maximum (HWHM) given by $\Gamma(q)$ and a diffusive peak at $\omega=0$ whose width is determined by the thermal diffusivity D_T. For a metallic system, D_T has electronic and ionic contributions with the former being dominant. However, it has been shown[52,53] that Eqs. (3) and (4) contain only the contribution to D_T due to the ions. The value of D_T predicted by fitting Eq. (3) to the low-q $F(q,t)$ values obtained in this work is $(1.0\pm0.3)\times10^{-3}$ cm^2/s, which is comparable to estimates made for the ionic contribution to D_T in liquid Si and Ge,[52,53] $\sim1.0\times10^{-3}$ and $\sim1.3\times10^{-3}$ cm^2/s, respectively (values that are about 2 orders of magnitude smaller than their respective total D_T values). The ionic contribution to D_T in liquid alkali metals near melting ranges from 20.0×10^{-3} cm^2/s (Li) to 3.0×10^{-3} cm^2/s (Cs).[54] Consequently, as D_T determines the diffusive behavior of $F(q,t)$ at small q's, the greater D_T values of the alkalis imply a smaller diffusive component that is easily overcome by the oscillatory parts of $F(q,t)$.

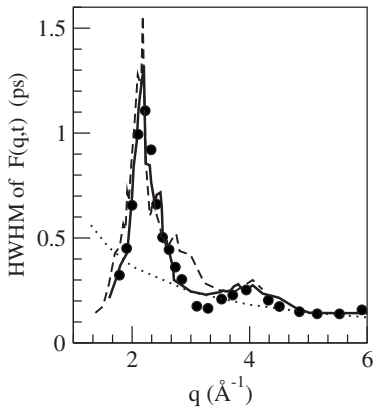

FIG. 5. Half width at half maximum (HWHM) of the intermediate scattering function $F(q,t)$. The solid and dashed lines represent our AIMD results $T=650$ K using relativistic and nonrelativistic pseudopotentials, respectively, and the solid circles represent the experimental data at 623 K (Ref. 27). The dotted line stands for the free particle limit.

The time decay of $F(q,t)$ is usually analyzed in terms of its HWHM. Figure 5 shows that the AIMD results we obtained using pseudopotentials with relativistic corrections closely follow the experimental INS data by Dahlborg *et al.*[27] for *l*-Pb at 623 K. By contrast, the results derived using nonrelativistic pseudopotentials are less satisfactory. In Fig. 5, we have also included the HWHM curve corresponding to the free particle limit, around which the two computed HWHM curves, and the curve joining the experimental data, exhibit an oscillatory behavior with phases resembling those of the corresponding $S(q)$ curves (Fig. 1). This close connection between the HWHM curves and the corresponding $S(q)$ curves is clearly evinced in the AIMD results obtained using the nonrelativistic pseudopotentials: the HWHM curve, besides exhibiting the same general pattern as its associated $S(q)$ curve, displays a singular feature at $q\sim3$ Å^{-1}, which is due to the shoulder in $S(q)$.

By a time FT of $F(q,t)$, we calculated the dynamic structure factor $S(q,\omega)$. However, as the present simulations lasted for 5.0 ps, for the smallest q values, i.e., for $q\leqslant0.5$ Å^{-1}, $F(q,t)$ was still significantly nonzero at the end of the simulation time, so that some caution had to be taken when performing its FT. This was carried out using an auxiliary window function that removes the cutoff noise in the FT of $F(q,t)$. The function is constant for small times and slowly decays to zero at the last considered point of $F(q,t)$. This approach provided well-behaved $S(q,\omega)$ (at the cost of a slight broadening and lowering of spectral side peaks). As a check of the reliability of the method used to compute $S(q,\omega)$, we resorted to the approach proposed by Ebbsjo *et al.*[48] Specifically, we took the FT of the result of fitting the calculated $F(q,t)$ with an eight-parameter analytical expres-

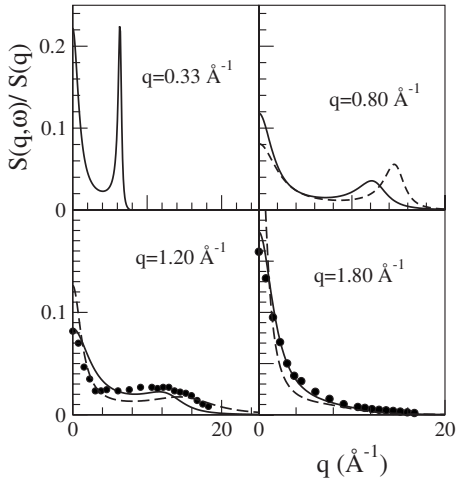

FIG. 6. Normalized dynamic structure factor $S(q,\omega)/S(q)$ of l-Pb for several values of q. The solid and dashed lines represent our AIMD results at $T=650$ K using relativistic and nonrelativistic pseudopotentials, respectively, and the solid circles represent the experimental INS data at 623 K (Ref. 25). For some values of q, the two sets of AIMD results are virtually the same.

sion that interpolates among the ideal gas, viscoelastic, and hydrodynamic models (see Fig. 4). The resulting dynamic structure factors were similar to those previously obtained, with the side peaks remaining at the same positions although somewhat higher.

Figures 6 and 7 show an illustrative sample of the computed dynamic structure factors $S(q,\omega)$ for different wave vectors up to $\sim 2q_p$. They have well defined side peaks, indicative of collective density excitations, up to $q \sim (3/5)q_p$; beyond this value, the side peaks become shoulders up to $q \sim 1.5$ Å^{-1}, and for larger q values, $S(q,\omega)$ shows a monotonically decreasing behavior. We stress that the existence of side peaks as well as its range of appearance are typical features of simple liquid metals.[28–32] Figures 6 and 7 also shows experimental results for the dynamic structure factor of l-Pb at $T=623$ K that were obtained by INS

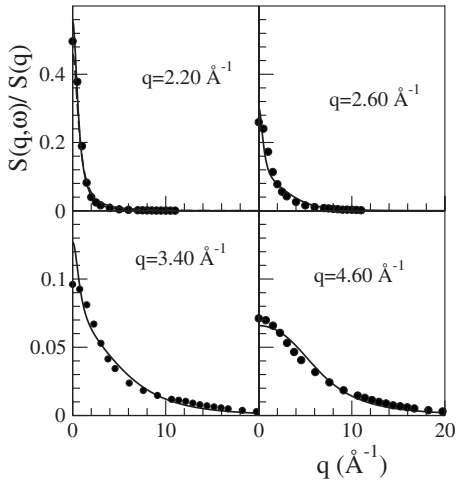

FIG. 7. As for Fig. 6, but for other values of q.

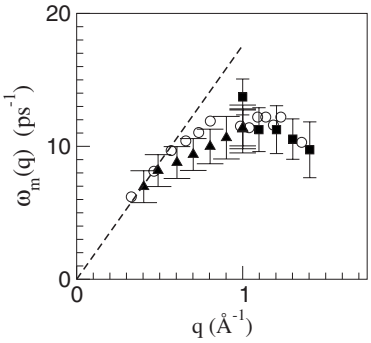

FIG. 8. Dispersion relation $\omega_m(q)$ for l-Pb. The open circles represent our AIMD results at $T=650$ K as obtained from the position of the side peaks in $S(q,\omega)$ using relativistic pseudopotentials. The solid triangles and squares, with error bars, correspond to INS data at $T=623$ K taken from Refs. 24 and 25, respectively. The dashed line is the linear dispersion with the experimental hydrodynamic adiabatic speed of sound $c_s=1760$ m/s (Ref. 55).

measurements.[25] Comparison with the computed $S(q,\omega)$ curves again shows that the AIMD predictions obtained using relativistic pseudopotentials are better than those obtained with nonrelativistic pseudopotentials.

From the position of the side peaks in the dynamic structure factors $S(q,\omega)$, we obtained the dispersion relation of the density fluctuations $\omega_m(q)$, which is shown in Fig. 8 together with available INS data[24,25] for l-Pb at $T=623$ K. For small q, the slope of the dispersion relation gives a q-dependent adiabatic speed of sound $c_s(q)$, which in the limit $q \to 0$ reduces to the bulk adiabatic speed of sound c_s. The value of c_s predicted by fitting a straight line to the low-q $\omega_m(q)$ values obtained in this work using relativistic pseudopotentials is 1750 ± 100 m/s, which agrees very well with the experimental data, ~ 1760 m/s.[55] c_s can also be obtained from the expression $c_s=[\gamma k_B T/mS(q \to 0)]^{(1/2)}$,[29] where m is the atomic mass. Using for the ratio of the specific heats the value $\gamma=1.20$ (Ref. 42) and our calculated value $S(q \to 0)=0.010$, the previous expression gives $c_s=1770 \pm 50$ m/s, which shows the consistency between the static and dynamic AIMD results obtained in the present work. The use of nonrelativistic pseudopotentials leads to a somewhat greater value of c_s, 1850 ± 100 m/s, a result that is consistent with the fact that the corresponding $S(q \to 0)$ value was smaller.

Our AIMD results shown in Fig. 8 do not reach small enough q values to allow a conclusive analysis of the possible existence of a positive dispersion, i.e., an increase of $\omega_m(q)$ with respect to the linear hydrodynamic dispersion relation. This phenomenon has been experimentally observed in liquid alkali metals,[56–58] as well as in liquid Al,[58] Mg,[59] and Hg.[60] Therefore, judging from the previously mentioned similarities among l-Pb and simple liquid metals, it seems plausible that l-Pb might also exhibit such a phenomenon.

Associated with the density fluctuations is the current due to the overall motion of the particles, defined as

$$\mathbf{j}(q,t) = \sum_a \mathbf{v}_a(t)\exp[i\mathbf{q}\cdot\mathbf{R}_a(t)]. \quad (5)$$

The longitudinal and transverse current correlation functions are, respectively, given by

$$C_L(q,t) = \langle j_L(q,t)j_L^*(q,0)\rangle \quad (6)$$

and

$$C_T(q,t) = \langle j_T(q,t)j_T^*(q,0)\rangle, \quad (7)$$

where $j_L(q,t)$ and $j_T(q,t)$ are the components of $\mathbf{j}(q,t)$ that are, respectively, longitudinal and transverse to $\mathbf{q}$. $C_T(q,t)$ is not directly associated with any measurable quantity but through MD simulations provides information on shear modes. In the free particle limit ($q\to\infty$), it is Gaussian with respect to both q and t, and in the hydrodynamic limit ($q\to 0$), it is Gaussian with respect to q and exponential with respect to t; for intermediate q values, $C_T(q,t)$ exhibits a more complicated behavior.[30] Its spectrum, $C_T(q,\omega)$, may show peaks within some q range, which are connected with the propagation of shear waves. The present AIMD calculations show that, for l-Pb at $T=650$ K, $C_T(q,\omega)$ displays peaks for a range $0.2q_p \leqslant q \leqslant 3q_p$, which is similar to the range found for simple liquid metals near melting.[30] The shear viscosity coefficient η can easily be obtained from $C_T(q,t)$, as indicated, for instance, in Refs. 30, 31, 61, and 62. Our AIMD calculations using relativistic pseudopotentials give $\eta=2.35\pm0.15$ GPa ps. The experimental value at melting is $\eta=2.61$ GPa ps,[63] which when extrapolated[63] to the temperature used in the present study, $T=650$ K, gives $\eta=2.30$ GPa ps. The use of nonrelativistic pseudopotentials leads to a value in worse agreement with experiment, $\eta=2.7\pm0.20$ GPa ps.

Within the context of the Brownian motion of a macroscopic particle of diameter d in a liquid of viscosity η, the Stokes-Einstein relation $\eta=k_BT/(2\pi dD)$ provides a connection between η and the self-diffusion coefficient D.[29] Although approximate when applied to atoms, this relation has been used to estimate η by identifying d with the position of the main peak of $g(r)$. When D is set equal to 0.215 Å^2/ps (the average of the two values obtained in this work using relativistic corrections, 0.21 and 0.22 Å^2/ps) and d to the position of the main peak of $g(r)$, $d=3.28$ Å, the value of η afforded by the Stokes-Einstein relation is 2.05 GPa ps. Although this result is somewhat smaller than that obtained above, it still supports the validity of using the Stokes-Einstein relation for atoms.

C. Density of states

Figure 9 shows the relativistic and nonrelativistic electronic DOS curves obtained for l-Pb at $T=650$ K. The DOS curve generated using relativistic pseudopotentials clearly shows a metallic behavior, a strong departure from the free-electron parabolic DOS curve, and a gap of about 2.3 eV separating a lower s-like and an upper p-like band, in keeping with the CMD predictions by Jank and Hafner[9] using an orthogonalized-plane-wave pseudopotential generated with relativistic core wave functions and the AIMD results by Knider *et al.*[14] The existence of such a gap is in agreement with conclusions drawn on the basis of photoemission spectra results (see Ref. 9 and references cited therein). By contrast, the DOS curve obtained using nonrelativistic pseudopotentials does not exhibit such a separation between states of different character. This shows that relativistic effects also play a fundamental role in determining the electronic structure of l-Pb. It should be noted that the electronic behavior of l-Pb is quite different from that obtained for a simple liquid metal such as l-Al, whose electronic DOS is quite close to the free-electron curve.[32]

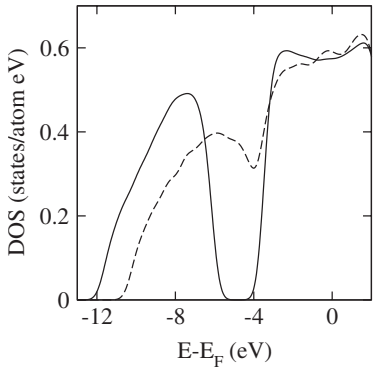

FIG. 9. Density of states (DOS) of l-Pb. The solid and dashed lines represent our AIMD results at $T=650$ K using relativistic and nonrelativistic pseudopotentials, respectively. The results were obtained by averaging over several ionic configurations and by sampling the Brillouin zone over eight special points.

IV. SUMMARY AND CONCLUSIONS

In this work, we compute the static, dynamic, and electronic properties of l-Pb at $T=650$ K, $\rho=0.0309$ Å^{-3} by means of 216-particle AIMD simulations based on PARSEC, a real-space pseudopotential approach based on DFT. The AIMD results that we obtain using relativistic pseudopotentials are in very good agreement with experiment for both static, dynamic, and electronic properties. By contrast, the results obtained using nonrelativistic pseudopotentials are less satisfactory. In particular, the use of nonrelativistic pseudopotentials produces a static structure that resembles more those of other, lighter, molten elements of group IV. The importance of including relativistic effects for an appropriate description of static and electronic properties of l-Pb was already highlighted by Jank and Hafner,[9] who performed CMD simulations using an effective inter-ionic pair potential derived from a nonlocal pseudopotential. In this work, this analysis, besides being performed using AIMD simulations rather than CMD simulations, has been extended to include the dynamic properties.

ACKNOWLEDGMENTS

This work was supported by the Spanish Ministry of Education and Science in conjunction with the European Regional Development Fund (Grants Nos. FIS2005-04239 and

MAT2005-03415). Computational support was provided by the Galician Supercomputing Center (CESGA) and the Barcelona Supercomputing Center (BSC). M.M.G.A. acknowledges support from the Spanish Ministry of Education and Science under the program "Ramón y Cajal". J.R.C. would like to thank support by the National Science Foundation under DMR-0551195 and the U.S. Department of Energy under DE-FG02-06ER46286 and DE-FG02-06ER15760.

[1] P. Hohenberg and W. Kohn, Phys. Rev. **136**, B864 (1964).
[2] W. Kohn and L. J. Sham, Phys. Rev. **140**, A1133 (1965).
[3] H. Hellmann, *Einführung in die Quantenchemie* (Deuticke, Leipzig, 1937); R. P. Feynman, Phys. Rev. **56**, 340 (1939).
[4] N. W. Ashcroft and J. Lekner, Phys. Rev. **145**, 83 (1966).
[5] J. M. Ziman, Philos. Mag. **6**, 1013 (1961).
[6] I. H. Umar and W. H. Young, J. Phys. F: Met. Phys. **4**, 525 (1974).
[7] P. Ascarelli, Phys. Rev. **173**, 271 (1968).
[8] R. Mentz-Stern and C. Hoheisel, Phys. Rev. A **40**, 4558 (1989).
[9] W. Jank and J. Hafner, Phys. Rev. B **41**, 1497 (1990).
[10] M. Dzugutov, K.-E. Larsson, and I. Ebbsjö, Phys. Rev. A **38**, 3609 (1988); K.-E. Larsson, W. Gudowski, and M. Dzugutov, *ibid.* **46**, 1132 (1992); W. Gudowski, M. Dzugutov, and K.-E. Larsson, Phys. Rev. E **47**, 1693 (1993).
[11] T. Bryk and I. Mryglod, Phys. Rev. E **63**, 051202 (2001); **64**, 032202 (2001).
[12] G. Kresse, J. Non-Cryst. Solids **312-314**, 52 (2002).
[13] T. Itami, S. Munejiri, T. Masaki, H. Aoki, Y. Ishii, T. Kamiyama, Y. Senda, F. Shimojo, and K. Hoshino, Phys. Rev. B **67**, 064201 (2003).
[14] F. Knider, J. Hugel, and A. V. Postnikov, J. Phys.: Condens. Matter **19**, 196105 (2007).
[15] G. Kresse and J. Furthmüller, Comput. Mater. Sci. **6**, 15 (1996); Phys. Rev. B **54**, 11169 (1996).
[16] J. P. Perdew, J. A. Chevary, S. H. Vosko, K. A. Jackson, M. R. Pederson, D. J. Singh, and C. Fiolhais, Phys. Rev. B **46**, 6671 (1992).
[17] J. M. Soler, E. Artacho, J. D. Gale, A. García, J. Junquera, P. Ordejón, and D. Sánchez-Portal, J. Phys.: Condens. Matter **14**, 2745 (2002).
[18] Y. Waseda, *The Structure of Non-Crystalline Materials* (McGraw-Hill, New York, 1980).
[19] D. M. North, J. E. Enderby, and P. A. Egelstaff, J. Phys. C **1**, 784 (1968).
[20] U. Dahlborg, M. Davidovic, and K. E. Larsson, Phys. Chem. Liq. **6**, 149 (1977).
[21] L. G. Olsson and U. Dahlborg, Phys. Chem. Liq. **11**, 225 (1982).
[22] P. A. Egelstaff, Acta Crystallogr. **7**, 673 (1954).
[23] B. N. Brockhouse, L. M. Corliss, and J. M. Hastings, Phys. Rev. **98**, 1721 (1955).
[24] O. Söderström, J. R. D. Copley, J.-B. Suck, and B. Dorner, J. Phys. F: Met. Phys. **10**, L151 (1980).
[25] O. Söderström, Phys. Rev. A **23**, 785 (1981).
[26] O. Söderström, U. Dahlborg, and M. Davidovič, Phys. Rev. A **27**, 470 (1983).
[27] U. Dahlborg, O. Söderström, W. Gudowsky, K. E. Larsson, and M. Davidovič, J. Phys. F: Met. Phys. **15**, 2053 (1985).
[28] J. P. Boon and S. Yip, *Molecular Hydrodynamics* (McGraw-Hill, New York, 1980).
[29] J. P. Hansen and I. R. McDonald, *Theory of Simple Liquids* (Academic, New York, 1986).
[30] U. Balucani and M. Zoppi, *Dynamics of the Liquid State* (Clarendon, Oxford, 1994).
[31] D. J. González, L. E. González, J. M. López, and M. J. Stott, J. Chem. Phys. **115**, 2373 (2001); Phys. Rev. B **65**, 184201 (2002).
[32] M. M. G. Alemany, L. J. Gallego, and D. J. González, Phys. Rev. B **70**, 134206 (2004).
[33] See http://www.ices.utexas.edu/parsec/
[34] See, for example, T. L. Beck, Rev. Mod. Phys. **72**, 1041 (2000).
[35] M. M. G. Alemany, M. Jain, L. Kronik, and J. R. Chelikowsky, Phys. Rev. B **69**, 075101 (2004); M. M. G. Alemany, M. Jain, M. L. Tiago, Y. Zhou, Y. Saad, and J. R. Chelikowsky, Comput. Phys. Commun. **117**, 339 (2007).
[36] N. Troullier and J. L. Martins, Phys. Rev. B **43**, 1993 (1991).
[37] L. Kleinman and D. M. Bylander, Phys. Rev. Lett. **48**, 1425 (1982).
[38] D. M. Ceperley and B. J. Alder, Phys. Rev. Lett. **45**, 566 (1980).
[39] J. P. Perdew and A. Zunger, Phys. Rev. B **23**, 5048 (1981).
[40] N. Binggeli, J. L. Martins, and J. R. Chelikowsky, Phys. Rev. Lett. **68**, 2956 (1992).
[41] D. Beeman, J. Comput. Phys. **20**, 130 (1976).
[42] M. Shimoji, *Liquid Metals* (Academic, New York, 1977).
[43] U. Balucani, A. Torcini, and R. Vallauri, Phys. Rev. A **46**, 2159 (1992); Phys. Rev. B **47**, 3011 (1993).
[44] M. M. G. Alemany, J. Casas, C. Rey, L. E. González, and L. J. Gallego, Phys. Rev. E **56**, 6818 (1997); J. Casas, D. J. González, and L. E. González, Phys. Rev. B **60**, 10094 (1999).
[45] M. Tanigaki, Y. Toyota, M. Harada, and W. Eguchi, J. Chem. Eng. Jpn. **16**, 92 (1983).
[46] S. Kambayashi and G. Kahl, Phys. Rev. A **46**, 3255 (1992); G. Kahl and S. Kambayashi, J. Phys.: Condens. Matter **6**, 10897 (1994).
[47] M. M. G. Alemany, C. Rey, and L. J. Gallego, Phys. Rev. B **58**, 685 (1998).
[48] I. Ebbsjo, T. Kinell, and I. Waller, J. Phys. C **13**, 1865 (1980).
[49] A. Torcini, U. Balucani, P. H. K. de Jong, and P. Verkerk, Phys. Rev. E **51**, 3126 (1995).
[50] F. Shimojo, K. Hoshino, and M. Watabe, J. Phys. Soc. Jpn. **63**, 141 (1994).
[51] J. Casas, D. J. González, and L. E. González, Phys. Rev. B **60**, 10094 (1999); J. Casas, D. J. González, L. E. González, M. M. G. Alemany, and L. J. Gallego, *ibid.* **62**, 12095 (2000).
[52] A. Delisle, D. J. Gonzalez, and M. J. Stott, Phys. Rev. B **73**, 064202 (2006); J. Phys.: Condens. Matter **18**, 3591 (2006).
[53] J.-D. Chai, D. Stroud, J. Hafner, and G. Kresse, Phys. Rev. B **67**, 104205 (2003).
[54] J. G. Cook and G. H. Fritsch, in *Handbook of Thermodynamic and Transport Properties of Alkali Metals*, edited by R. W. Oshe (Blackwell, Oxford, 1985).
[55] R. B. Gordon, Acta Metall. **7**, 1 (1959).

[56] H. Sinn and E. Burkel, J. Phys.: Condens. Matter **8**, 9369 (1996); H. Sinn, F. Sette, U. Bergmann, Ch. Halcoussis, M. Krisch, R. Verbeni, and E. Burkel, Phys. Rev. Lett. **78**, 1715 (1997).
[57] W.-C. Pilgrim, S. Hosokawa, H. Saggau, H. Sinn, and E. Burkel, J. Non-Cryst. Solids **250**, 96 (1999).
[58] T. Scopigno, U. Balucani, G. Ruocco, and F. Sette, Phys. Rev. E **63**, 011210 (2000).
[59] Y. Kawakita, S. Hosokawa, T. Enosaki, K. Ohshima, S. Takeda, W.-C. Pilgrim, S. Tsutsui, Y. Tanaka, and A. Q. R. Baron, J. Phys. Soc. Jpn. **72**, 1603 (2003).
[60] S. Hosokawa, H. Sinn, F. Hensel, A. Alatas, E. E. Alp, and W. C. Pilgrim, J. Non-Cryst. Solids **312**, 163 (2002).
[61] B. J. Palmer, Phys. Rev. E **49**, 359 (1994).
[62] U. Balucani, J. P. Brodholt, P. Jedlovszky, and R. Vallauri, Phys. Rev. E **62**, 2971 (2000).
[63] M. Shimoji and T. Itami, *Atomic Transport in Liquid Metals* (Trans. Tech., Switzerland, 1986).